Accepted Manuscript

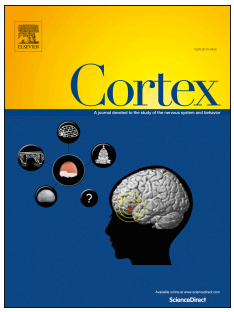

Time-resolved decoding of planned delayed and immediate prehension movements

Giacomo Ariani, Nikolaas N. Oosterhof, Angelika Lingnau

PII: S0010-9452(17)30415-X

DOI: 10.1016/j.cortex.2017.12.007

Reference: CORTEX 2205

To appear in: *Cortex*

Received Date: 10 July 2017

Revised Date: 20 October 2017

Accepted Date: 11 December 2017

Please cite this article as: Ariani G, Oosterhof NN, Lingnau A, Time-resolved decoding of planned delayed and immediate prehension movements, *CORTEX* (2018), doi: 10.1016/j.cortex.2017.12.007.

TITLE

Time-resolved decoding of planned delayed and immediate prehension movements

AUTHOR NAMES AND AFFILIATIONS

Giacomo Ariani[1]*, Nikolaas N. Oosterhof[1], Angelika Lingnau[1,2,3]

[1]Center for Mind/Brain Sciences (CIMeC), University of Trento, Italy

[2]Department of Psychology & Cognitive Science, University of Trento, Italy

[3]Department of Psychology, Royal Holloway University of London, United Kingdom

***CORRESPONDING AUTHOR**[4]

Giacomo Ariani, PhD

Center for Mind/Brain Sciences (CIMeC), University of Trento

Corso Bettini 31, 38068, Rovereto (TN), Italy

giacomo.ariani@gmail.com

[4]**PRESENT ADDRESS**

The Brain and Mind Institute, Western University

1151 Richmond Street, N6A 3K7, London (ON), Canada

gariani@uwo.ca

CONTENTS OF MANUSCRIPT

Number of pages: 36

Number of figures: 6

Number of supplementary figures: 3

Number of tables: 1

Abstract word count: 189 / 300

AUTHOR CONTRIBUTIONS

G.A., N.N.O., and A.L. designed research; G.A. performed research; G.A. and N.N.O. analyzed data; G.A., N.N.O., and A.L. wrote the manuscript.

ABSTRACT

Different contexts require us either to react immediately, or to delay (or suppress) a planned movement. Previous studies that aimed at decoding movement plans typically dissociated movement preparation and execution by means of delayed-movement paradigms. Here we asked whether these results can be generalized to the planning and execution of immediate movements. To directly compare delayed, non-delayed, and suppressed reaching and grasping movements, we used a slow event-related functional magnetic resonance imaging (fMRI) design. To examine how neural representations evolved throughout movement planning, execution, and suppression, we performed time-resolved multivariate pattern analysis (MVPA). During the planning phase, we were able to decode upcoming reaching and grasping movements in contralateral parietal and premotor areas. During the execution phase, we were able to decode movements in a widespread bilateral network of motor, premotor, and somatosensory areas. Moreover, we obtained significant decoding across delayed and non-delayed movement plans in contralateral primary motor cortex. Our results demonstrate the feasibility of time-resolved MVPA and provide new insights into the dynamics of the prehension network, suggesting early neural representations of movement plans in the primary motor cortex that are shared between delayed and non-delayed contexts.

Key words: delayed-movement paradigm; immediate movements; movement planning; prehension network; time-resolved fMRI-MVPA.

1. INTRODUCTION

Our actions vary with context. While certain situations demand an immediate response, others require to withhold movements until the right moment. Finally, some situations require getting prepared for, but then refraining from moving at all. How does the human brain exercise control on our actions in different contexts? Unlike motor reflexes, even relatively simple voluntary movements need to be prepared before they are executed (Haggard, 2005, 2008). Understanding how specific brain areas contribute to movement planning requires being able to dissociate planning-related from movement-related activity. To do so, previous monkey (Cisek and Kalaska, 2004, 2005, Churchland et al., 2006, 2010; Baumann et al., 2009; Hwang and Andersen, 2009; Fluet et al., 2010; Afshar et al., 2011; Cui and Andersen, 2011; Townsend et al., 2011) and human studies (e.g., Toni et al., 2001; Mars et al., 2008; Gallivan et al., 2011b; Ariani et al., 2015; Gertz and Fiehler, 2015) typically adopted delayed-movement paradigms in which arm or eye movements are planned and withheld in memory (often for several seconds, especially in human fMRI studies) before being released upon the presentation of a trigger cue. During planning delays, these studies revealed widespread cortical activation in a number of frontal (e.g., premotor, motor, and supplementary motor areas) and parietal (e.g., somatosensory and visuomotor areas) regions showing preferences for spatial target locations (Lindner et al., 2010; Pertzov et al., 2011), movement effectors (e.g., hand, eyes, foot; Heed et al., 2011; Leoné et al., 2014), different prehension movements (Raos, 2004; Verhagen et al., 2008, 2012, 2013) or sensory modalities (e.g., visual vs haptic; Beurze et al., 2009). More recently, a number of studies demonstrated that delay-related brain responses from the aforementioned parieto-frontal regions can be analyzed to predict several action-related parameters (e.g., effector choice, target location, movement direction, grip type) of upcoming prehension movements (for a review, Gallivan and Culham, 2015).

Memory-guided (i.e., delayed) and immediate (i.e., non-delayed) actions have been suggested to rely on areas of the ventral and dorsal visual streams, respectively (Hu et al., 1999; Goodale et al., 2004; Singhal et al., 2013; however see Himmelbach et al., 2009; Fiehler et al., 2011 for an opposing view). This raises the question whether results obtained from paradigms that typically use long planning delays (> 10 s) to separate planning and

execution can be generalized to the planning of immediate actions. Another possible limitation of the delayed-movement approach lies in the difficulty of disentangling processes co-occurring with movement planning (such as verbal working memory, sensory event anticipation, mind wandering, etc.) during the delay period. Similarly, Ames et al. (2014) argued that, during the delay, subjects are not only planning but also actively withholding a movement. To clarify the neuronal relationship between memory-guided and immediate movements and identify a neural correlate of early planning stages (e.g., selection of response parameters such as movement direction or amplitude) that is not contaminated by either delay- or execution-related processes, Ames et al. (2014) recorded from neurons in the dorsal premotor cortext (PMd) and primary motor cortex (M1) while macaques performed delayed and non-delayed reaching movements in separate blocks of trials. Corroborating previous results (Crammond and Kalaska, 2000), the authors found that responses of neuronal populations to the instruction cue of delayed movements and to the go cue of non-delayed movements (prior to movement onset) were highly similar across the delayed and non-delayed conditions. Following up on these results, we asked whether multivariate decoding of planned prehension movements obtained with a delayed-movement paradigm can be generalized to the preparation of immediate prehension movements in humans. To address this question, we carried out an fMRI experiment in which reaching or grasping movements were performed under three main conditions: (1) a *delayed task*, which included jittered delays between planning and execution (delayed go); (2) a *non-delayed task*, in which participants had to immediately execute the instructed movement without any additional delay (non-delayed go); and (3) a *no-go task* that was identical to the delayed task but ended with a no-go cue indicating to suppress the previously instructed movement (delayed no-go). The *no-go task* had the double function to further discourage movement anticipation, and to ensure that neural responses to movement planning were not always followed (and thus systematically contaminated) by movement execution. To better separate the sensory and motor contributions to movement planning, movements were performed without visual feedback of the target object, or the moving limbs (i.e., non visually-guided movements; for a similar approach see Fabbri et al., 2010, 2012, 2014; Ariani et al., 2015). Given the short temporal window for the planning of immediate movements, to test whether multi-voxel

patterns obtained during the planning phase of delayed movements show similarities with those obtained for non-delayed movements, we performed multivariate pattern analysis (MVPA) of fMRI data using a time-resolved approach (i.e., decoding separately for each acquired volume). To disambiguate the decoding of cues from the decoding of motor plans during cross-condition decoding (i.e., training a classifier on delayed movement planning and using independent data from non-delayed execution for testing, and vice versa), instructing cues were delivered in different sensory modalities for the *delayed task* (i.e., visual cues) and the *non-delayed task* (i.e., auditory cues). The combination of this method with our design allowed us to (1) examine the time course of movement decoding (i.e., how movement representations evolve throughout the planning phase in different regions of the human prehension system); (2) identify shared neural representations across delayed and non-delayed movement plans; (3) explore whether regions recruited during movement suppression (*no-go task*, after the no-go cue) carry information about the previously formed and then inhibited movement plans.

2. MATERIALS AND METHODS

2.1 Participants. We recruited twenty-four right-handed volunteers (11 males, 13 females; mean age: 28.21 years; age range: 18-38 years). All participants were neurologically intact and had either normal or corrected-to-normal vision. Participants gave written informed consent and were paid €30 for their participation. The experimental procedures were approved by the ethics committee of the University of Trento.

2.2 Setup. Visual stimuli were back-projected to a screen (frame rate: 60 Hz; screen resolution: 1280 × 1024 pixels) via a liquid crystal projector (OC EMP 7900, Epson Nagano, Japan). Participants viewed the screen binocularly through an angled mirror mounted on the head coil (Fig. 1 A). Auditory cues were delivered via standard MR-compatible headphones. Participants were scanned in a conventional fMRI configuration (i.e., lying horizontally, without tilting the head towards the body) and were required to maintain fixation (Fig. 1 A). This setup prevented uncontrolled visual feedback from the sight of their own limbs and the target object, or systematic eye movements towards limbs or the target object, while performing the task (Fabbri et al., 2014; Ariani et al., 2015). The workspace consisted of a transparent plexiglas board attached to the scanner bed at waist level (Fig. 1 A-B). We instructed participants to perform unimanual right-handed movements towards a custom-made target object placed on the workspace and located centrally with respect to the participant's sagittal midline. While at rest, participants were instructed to keep their right hand closed in a fist relaxedly pressing the keys (home position) of a button box (Lumina LP 400, Cambridge Research Systems) attached to a custom-made belt around their waist. A microcontroller board (Arduino Uno) connected to the Lumina Controller positioned outside the magnet room was used to signal the release of the keys at movement onset. This time stamp was used to define and measure reaction times (RTs). To allow movements to be as comfortable as possible, the position of the workspace and the button box were adjusted individually to match each participant's arm length (mean distance hand-object: 15.88 ± 2.25 cm). Head and trunk movements were minimized by stabilizing the head and the upper right arm with foam blocks and cushions. To control for task execution, we recorded each experimental session using an MR-compatible digital video camera (VP-D15i; Samsung Electronics) placed on a tripod in a corner of the

scanner room (outside the 0.5 mT line). Stimulus presentation, response collection, and synchronization with the scanner were controlled using *ASF* (Schwarzbach, 2011), based on the Matlab Psychtoolbox 3 for Windows (Brainard, 1997).

< Fig. 1, 2 columns >

2.3 Experimental design and timing. To compare delayed, non-delayed and suppressed movement plans, we used a slow event-related design with factors *movement type* (reach-to-touch, T; reach-to-grasp, G; Fig. 1 B) and *task* (delayed go, D; non-delayed go, ND; delayed no-go, NG; Fig. 1 C). Both factors were pseudo-randomized within each experimental run. A brief change in brightness of the grey fixation cross (alert cue, 500 ms) informed participants about the beginning of each trial and an upcoming cue. Importantly, the alert cue was always the same and presented before each trial type and thus was not informative with respect to any task or movement type. Its purpose was simply to keep participants engaged in the task throughout the experiment. In the delayed task (Fig. 1 C, top row), the alert cue was immediately followed by a change in color of the fixation cross (color cue, 500 ms) instructing which of the two movements to prepare (e.g., green fixation cross = reach-to-touch; yellow fixation cross = reach-to-grasp). We asked participants to start preparing for the instructed movement right after the presentation of the color cue (planning phase), and then to wait until the appearance of the go cue (darkening of the fixation cross) to execute the movement. A variable delay of 8 to 14 seconds (in steps of the TR, 2 s) preceded the go cue. In each run, for tasks with a delay (i.e., delayed go and delayed no-go), each delay duration (i.e., 8 s, 10 s, 12 s, 14 s) preceded each factorial combination of movement type and task four times (i.e., 2 movement types x 2 delayed tasks x 4 delay durations = 16 delayed trials per run). The go cue was presented for 2s, ensuring enough time to start and complete the instructed movement to the target object (execution phase). Participants were instructed to react as soon as the go cue appeared, but also encouraged to prioritize accuracy over speed. After movement completion, participants had to keep their hand on the target object until the fixation cross returned to the initial grey color (go-back cue), and then to return to the home position (see *Setup*). The reason for a go-back cue was to ensure that the timing of the return

movement was comparable across participants. In the non-delayed task (Fig. 1 C, middle row), following the alert cue, an auditory cue (*'beep'*, 300 ms) presented simultaneous to the go cue (darkening of the fixation) indicated which movement to perform (high-pitch sound, 650 Hz = reach-to-touch; low-pitch sound, 250 Hz = reach-to-grasp). For this task participants, were asked to prepare and execute movements immediately (i.e., no delay between auditory instruction and go cue), and to remain on the target object until the go-back cue. Finally, during no-go trials (Fig. 1 C, bottom row), the delay (planning phase) was followed by a no-go cue (a red fixation cross, 500 ms), indicating to withhold the previously instructed movement and to remain as still as possible at the home position while waiting for the next trial to start. To keep participants focused throughout the experiment and to prevent psychological effects of task habituation or event anticipation with increasing number of trials, we included a small proportion of catch trials (~15%, 4 per run, 2 per movement) for the delayed task only, in which the delay duration was sensibly shorter (from 2 s to 6 s, in steps of 2 s, randomly sampled from a geometric distribution with $p = 0.3$). We subsequently excluded these trials from successive analyses. Each run started and ended with 12 s rest and contained 4 repetitions per factorial combination of movement type x task, plus catch trials (i.e., 24 + 4 = 28 trials per run; 280 trials per participant). The stimulus-response (S-R) mapping between cues (i.e., colors and sounds) and movements were counterbalanced across participants. Trial randomization and inter-trial-interval (ITI) jittering was determined using Optseq2 (Greve, 2002; available online at: http://surfer.nmr.mgh.harvard.edu/optseq). Each experimental session consisted of: training outside the MR scanner and setup preparation (~25 min), structural scan (~5 min), main experiment (10 functional runs, ~7 min each), for a total of ~100 min per participant. At the end of the session, participants filled out a post-session questionnaire to judge their wakefulness/concentration during the experiment, and any strategies they may have used during each of the tasks.

2.4 Data acquisition. Functional and structural data were collected using a 4T Bruker MedSpec Biospin MR scanner and an 8-channel birdcage head coil. Functional images were acquired with a T2*-weighted gradient-recalled echo-planar imaging (EPI) sequence. Acquisition parameters were a TR (time to repeat) of 2000 ms; voxel resolution, 3 x 3 x 3

mm^3; TE (time to echo), 28 ms; flip angle (FA), 73°; field of view (FOV), 192 x 192 mm^2; gap size, 0.45 mm. We used 30 slices, acquired in ascending interleaved order, slightly tilted to run approximately parallel to the calcarine sulcus. The number of volumes acquired in the main experiment for each functional run varied according to the length of variable delay periods (range: 190-200 volumes). Before each functional run, we performed an additional brief scan to measure the point-spread function (PSF) of the acquired sequence, which served to correct distortion to be expected with high-field imaging (Zaitsev et al., 2004). To be able to coregister the low-resolution functional images to a high-resolution anatomical scan, we acquired a T1-weighted anatomical scan (magnetization-prepared rapid-acquisition gradient echo; TR: 2700 ms; voxel resolution: 1 x 1 x 1 mm^3; TE: 4.18 ms; FA: 7°; FOV: 256 x 224 mm^2; 176 slices; generalized autocalibrating partially parallel acquisition with an acceleration factor of 2; inversion time: 1020 ms).

2.5 Data analysis.

2.5.1 Behavior. Reaction times (RTs) were measured as the time to release the response buttons (see *Setup*) with respect to the go cue. Video recordings of the experimental sessions were analyzed offline to ensure that participants had performed the movements correctly. Trials were considered errors either when performed incorrectly (i.e., imprecise hand preshaping; temporal anticipation: RT < 100 ms; reaction time timeout: RT > 1500 ms) or when participants executed a movement that was different from the one instructed by the visual or auditory cues. Error trials were excluded from all successive analyses.

2.5.2 fMRI preprocessing. Data were preprocessed and analyzed using BrainVoyager QX 2.8.0 (BrainInnovation, Maastricht, The Netherlands) in combination with the NeuroElf v1.0 toolbox and custom software written in Matlab R2012b (MathWorks, Natick, MA, U.S.A.). To correct for distortions in geometry and intensity in the echo planar imaging (EPI) images, we applied distortion correction on the basis of the PSF (see *Data acquisition;* Zeng & Constable, 2002). To avoid T1 saturation, we discarded the first 4 volumes of each run. The first volume of the first functional run of each participant was aligned to the high-resolution anatomy (6 rigid-body transformation parameters). Next, we performed 3D motion correction (trilinear

interpolation for estimation and sinc interpolation for resampling) using the first volume of the first run of each participant as reference, followed by slice timing correction (ascending interleaved even-odd order) and high-pass temporal filtering (3 cycles per run). Spatial smoothing was applied with a Gaussian kernel of 3 mm full-width half maximum (FWHM) for univariate and multivariate analyses. For successive group analysis, both functional and anatomical data were transformed into Talairach space, using trilinear interpolation.

2.5.3 Brain segmentation and surface mesh reconstruction. We used BrainVoyager to reconstruct individual surface meshes for each hemisphere of each subject along the border between grey and white matter. Next, separately for the left and right hemisphere, we combined the individual reconstructions of folded surfaces of all participants (N = 24) using cortex-based alignment as implemented in BrainVoyager QX 2.8.0. Group-aligned left and right hemisphere meshes were used to display statistical maps resulting from both uni- and multivariate second-level analyses.

2.5.4 Univariate RFX-GLM analysis. To examine the blood-oxygen level-dependent (BOLD) response during the three tasks, we ran a group random-effects (RFX) general linear model (GLM) analysis (N = 24; Supplementary Fig. 1). We created predictors for each factorial combination of movement type x task. Additionally, for tasks with a delay (i.e., delayed go and delayed no-go), we used separate predictors for movement planning (time-locked to the instructing cue) and movement execution/suppression (time-locked to the go/no-go cue). This resulted in a total of 10 predictors of interest: delayed planning/execution of touch/grasp (4), no-go planning/suppression of touch/grasp (4), non-delayed execution of touch/grasp (2). Each predictor was modeled with a standard duration of 1 s and convolved with the canonical hemodynamic response function (HRF). In addition, catch trials, error trials (collapsed across movement type, task, and phase [planning/execution]; i.e. one single error predictor) and 3D motion correction parameters (x, y, z translation and rotation) were included in the model as nuisance regressors. To identify brain regions involved in the preparation of prehension movements irrespective of whether the movement plan was subsequently executed or not we contrasted the planning phase of both go and no-go trials (collapsed across the two

movement types) against baseline (Supplementary Fig. 1 A). Similarly, to identify brain regions recruited during movement planning and execution, we contrasted the execution phase in the non-delayed task (collapsed across both movement types) against baseline (Supplementary Fig. 1 B). Finally, to examine whether any brain regions responded more strongly during no-go in comparison to go trials, we computed the contrast delayed no-go vs delayed go trials (Supplementary Fig. 1 C). The resulting volumetric statistical maps were corrected for multiple comparisons using Threshold Free Cluster Enhancement (TFCE, corrected $p < 0.05$, using Montecarlo permutations with 10.000 iterations) as implemented in the CoSMoMVPA v1.1 toolbox for Matlab/GNU Octave (Oosterhof et al., 2016), and projected on the group-averaged surface mesh for visualization purposes.

2.5.5 ROI definition. We defined regions of interest (ROIs) on the basis of a combination of anatomical and functional criteria using a similar procedure as in Ariani et al. (2015). First, on the group-averaged surface mesh we manually outlined bilateral ROIs around anatomical landmarks known to be involved in the planning and execution of prehension movements (Fig. 2), using the following anatomical criteria:

- *Dorsolateral prefrontal cortex (dlPFC)*: on the anterior portion of the middle frontal gyrus, around Brodmann area (BA) 46 (Badre & D'Esposito, 2009);
- *Ventral premotor cortex (PMv)*: slightly inferior and posterior to the junction of the inferior frontal sulcus and the precentral sulcus (Gallivan et al., 2011a);
- *Dorsal premotor cortex (PMd)*: at the junction of the superior frontal sulcus and the precentral sulcus;
- *Supplementary motor area (SMA)*: on the medial wall of the superior frontal gyrus, anterior to the medial end of the central sulcus, posterior to the vertical projection of the anterior commissure;
- *Primary motor cortex (M1)*: around the hand knob area in the anterior bank of the central sulcus;
- *Anterior intraparietal sulcus (aIPS)*: on the anterior segment of the intraparietal sulcus, at the junction with the postcentral sulcus;

- *Superior parietal lobule (SPL)*: the middle portion of the superior parietal lobule, superior to the IPS and posterior to the postcentral sulcus;
- Superior parieto-occipital cortex (SPOC): the posterior portion of the superior parietal lobule (Brodmann area 7b), located medially, superior to the IPS and anterior to the parieto-occipital sulcus (Scheperjans et al., 2008; Gallivan et al., 2011b);
- *Lateral occipito-temporal cortex (LOTC)*: covering the posterior middle temporal gyrus (pMTG), inferior to the superior temporal sulcus (STS) and anterior to the lateral occipital sulcus (LOS) (Lingnau and Downing, 2015).

Next, we projected these marked patches from the surface back to the volume. Within each, we looked for individual peak voxels resulting from the single-subject GLM contrasts [planning + execution > baseline], computed as described above. Finally, we defined individual ROIs, separately for each participant, as spheres (10 mm radius, ~230 voxels) centered around each individual peak voxel (for Talairach coordinates of individual ROIs, see Table 1).

Table 1. TAL coordinates (x, y, z rounded mean and standard deviation across participants) of individual peak voxels for the regions of interest (ROIs) identified by the group contrast [delayed planning + non-delayed execution > baseline].

Region	x	y	z	SD x	SD y	SD z
L-dlPFC	-34	33	32	4,7	4,1	3,5
R-dlPFC	31	35	32	3,1	3,8	3,6
L-PMv	-44	1	30	4,6	2,8	3,6
R-PMv	40	2	33	4,2	2,4	2,3
L-PMd	-27	-11	52	3,9	3,1	4,0
R-PMd	27	-10	52	3,2	4,0	4,7
L-SMA	-4	-11	53	1,0	3,5	2,9
R-SMA	6	-5	52	2,3	2,8	2,6
L-M1	-33	-24	50	2,3	2,9	1,9
R-M1	35	-22	50	2,8	3,1	2,3
L-aIPS	-39	-35	38	3,5	3,5	2,3

R-aIPS	35	-37	40	3,8	3,7	2,6
L-SPL	-27	-55	55	2,8	4,4,	3,3
R-SPL	29	-52	57	1,7	5,6	3,3
L-SPOC	-6	-71	43	2,7	3,0	3,9
R-SPOC	8	-70	43	2,7	3,1	4,5
L-LOTC	-43	-63	4	3,3	2,3	2,9
R-LOTC	49	-54	3	4,3	3,2	3,7

Abbreviations: L-, left hemisphere; R-, right hemisphere; dlPFC, dorsolateral prefrontal cortex; PMv, ventral premotor cortex; PMd, dorsal premotor cortex; SMA, supplementary motor area; M1, primary motor cortex; aIPS, anterior intraparietal sulcus; SPL, superior parietal lobule; SPOC, superior parieto-occipital cortex; LOTC, lateral occipito-temporal cortex.

< Fig. 2, 1.5 columns >

2.5.6 Time-resolved ROI-MVPA. To track the temporal unfolding of decoding of movement type for different brain regions and tasks, we used a time-resolved decoding approach (Fig. 3; Soon et al., 2008; Bode and Haynes, 2009; Harrison and Tong, 2009; Linden et al., 2012; Gallivan et al., 2013c) for both ROI- and searchlight-based MVPA. The ROI analysis (Fig. 4-6) was intended to examine previously reported regions known to play a role during planning and execution of prehension movements. The whole-brain searchlight analysis (Supplementary Fig. 2-3) was carried out to prevent missing potentially important regions not covered in the ROI analysis. Both analyses were performed in volume space and projected on group-aligned surface reconstructions for visualization purposes. To implement the time-resolved ROI-MVPA we repeated the following steps separately for each run of each participant and ROI (Fig. 3). First, for each voxel included in the ROI, we normalized the raw volume time-course (VTC) by subtracting the mean across all volumes. Next, for each factorial combination of movement type x task, we extracted K volumes starting from the onset of the condition (e.g., K = 5 volumes for delayed planning), separately for each run and participant (Fig. 3 A). For the planning phase in the delayed task and the cross-condition decoding, we selected 5 volumes from the onset of the instructing cue. The reason for this choice was that all delayed trials had a minimum delay of at least 8 s (see *2.3 Experimental design and timing*). Therefore the planning and execution of the same trial would not begin to

overlap at least until vol. 5 for trials with a 8 s delay, until vol. 6 for trials with a 10 s delay, until vol. 7 for trials with a 12 s delay, and until vol. 8 for trials with a 14 s delay. For the execution phase of both delayed and non-delayed tasks, and for the suppression in the no-go task, we selected 7 volumes to show the full development of decoding time course. For each classification pair (e.g., reach-to-touch vs reach-to-grasp, within the planning phase) this procedure resulted in a dataset matrix of samples [volumes (e.g., 5) x movement types (2) x runs (10)] x features [voxels in the ROI (~230)] for each participant, task and ROI (Fig. 3 B). In each matrix, the rows constituted the different multi-voxel patterns of fMRI data for each volume of each run for each movement type; the columns constituted data for each voxel in the ROI, from multiple volumes, movement types, and runs. Classification accuracies were computed separately for each volume (i.e., movements (2) x runs (10) = 20 patterns) using a leave-one-run-out cross-validation method (Fig. 3 C): a regularized linear discriminant analysis (LDA) classifier was trained on 18 patterns (2 movements x 9 runs) and tested on the data from the remaining run (2 patterns, one per movement type). The LDA classifier was regularized by adding to the covariance matrix the identity matrix scaled by one percent of the mean of the diagonal of the covariance matrix. Training and testing was repeated for 10 iterations, using all possible combinations of train and test runs. The average across these 10 iterations constituted the mean classification accuracy of the two movements per participant per ROI (Fig. 3 D). To test for representations of planned movements across the delayed and non-delayed conditions, we carried out cross-condition decoding: we trained the classifier on discriminating between reaching and grasping in one task (e.g., delayed planning) and tested the performance of the classifier to distinguish between reaching and grasping in the other task (e.g., non-delayed execution), and vice versa. Results from the two cross-condition decoding analyses were successively averaged to produce one score per cross-condition decoding. To assess statistical significance of the decoding accuracy, separately for each ROI, we performed one-sample *t*-tests on decoding accuracies across participants against chance decoding (50%) at each time-point. We ensured that chance level was 50% even after excluding error trials by balancing the cross-validation scheme such that for each fold, the training and test set consisted of the same number of patterns for each movement type. Statistical results were corrected for multiple comparisons (number of ROIs x time-points)

using TFCE (p < 0.05, 10.000 iterations) as implemented in CoSMoMVPA v1.1 (Oosterhof et al., 2016). Note that using BOLD time-course data as input for the classifier (e.g., instead of beta-weights or *t*-values coming from a first-level GLM analysis) made our findings less dependent on assumptions about the shape of the hemodynamic response function (HRF).

< Fig. 3, 2 columns >

2.5.7 Time-resolved searchlight-based MVPA. Decoding procedures for the exploratory time-resolved whole-brain searchlight analysis in the volume were nearly identical to the ones used for the ROI analysis. The main difference was that we used a spherical searchlight (~250 voxels) approach applied to each voxel of the entire brain instead of predefined ROIs; decoding results for each searchlight were assigned to the central voxel. Resulting group mean decoding accuracy maps at each time-point were then projected onto the group-aligned cortical surface mesh (see section *2.5.3 Brain segmentation and surface mesh reconstruction*) for visualization purposes (Supplementary Fig. 2-3, top rows). To identify voxels where classification was significantly greater than chance (50%) we performed a two-tailed one-sample *t*-test across individual whole-brain maps. Statistical *t*-maps were then corrected for multiple comparisons using TFCE (1000 iterations) as implemented in CoSMoMVPA (Oosterhof et al., 2016). Moreover, for descriptive purposes, we thresholded the uncorrected *t*-maps at t = 2 and marked significant clusters that survived TFCE correction with black outlines (Supplementary Fig. 2-3, bottom rows). Cluster-based TFCE was carried out using a neighborhood in which clusters could form along the spatial dimensions (i.e., voxels sharing an edge) but not along the temporal dimension (i.e., the neighborhood along the temporal dimension is a *singleton* neighborhood, and every feature is only neighbor to itself). This means that inferences about significance can be made at the single volume level along the temporal dimension (i.e. whether decoding is above chance at a specific time point, but not whether decoding at volume N is greater than at volume N-1). Regarding the spatial dimension, interferences about significance can be made at the level of clusters of voxels or ROIs, but not at the single voxel level. We created whole-brain *t*-maps and decoding accuracy

maps at each time-point, separately for the three tasks (within-condition decoding), and for the decoding across delayed planning and non-delayed execution (cross-condition decoding).

3. RESULTS

3.1 Behavior. Participants responded substantially faster in the delayed (660.48 ± 11.54 ms) compared to the non-delayed task (905.54 ± 12.83; $t(23) = -9.58$, $p < 0.0001$), suggesting a benefit of having time to prepare during the delay/planning phase. Error rates were low and comparable for the delayed (7.39% ± 1.48) and the non-delayed task (6.25% ± 1.55; signed-rank $z(23) = 0.78$, $p = 0.43$), possibly reflecting successful training before the scanning session and the participants' focus on accuracy over speed. In the no-go task participants made an average of 0.42% ± 0.18 *false start* errors (i.e., go cue anticipation).

3.2 fMRI.

3.2.1 Univariate RFX-GLM analysis. We used a univariate RFX-GLM analysis to identify brain regions recruited during movement planning, execution and suppression (for details, see Materials and Methods, section *2.5.4 Univariate RFX-GLM analysis*). First, the contrast [delayed planning > baseline] (Supplementary Fig. 1 A) revealed a widespread bilateral network of frontal, parietal and temporal regions, in line with previous studies (Gallivan et al., 2011a, 2011b; Brandi et al., 2014; Leoné et al., 2014; Ariani et al., 2015; Gertz and Fiehler, 2015). Second, the contrast [non-delayed execution > baseline] (Supplementary Fig. 1 B) revealed a network of areas comparable to that involved in movement planning. As expected, in comparison to the statistical map resulting from the contrast [delayed planning > baseline], the statistical map resulting from the contrast [non-delayed execution > baseline] was more widespread and showed considerably stronger effects in primary motor and auditory areas (likely due to the auditory cues instructing which movement to perform in this task). Third, the contrast [delayed no-go > delayed go] (Supplementary Fig. 1 C) did not reveal any areas that survived TFCE. As expected, the reverse contrast [delayed go > delayed no-go] showed a widespread network of areas comparable to those recruited during movement planning and execution.

To define a set of group ROIs in areas known to be recruited during movement planning and execution for the time-resolved within- and cross-condition decoding analysis, we computed the contrast [delayed planning + non-delayed execution > baseline] (Fig. 2). Note that we chose this contrast to prevent biasing the decoding analysis towards planning- or execution-

related areas, which is relevant in particular for the cross-decoding analysis. At the same time, this contrast does not introduce any bias towards one of the two movement types (or the contrast between the two) and thus prevents circular analysis (Kriegeskorte et al., 2009). On the basis of this contrast, we selected 18 bilateral frontal, parietal and temporal ROIs individually for each participant (see section *2.5.5 ROI definition* and Table 1): left and right dorsolateral prefrontal cortex (dlPFC); left and right ventral premotor cortex (PMv); left and right dorsal premotor cortex (PMd), left and right supplementary motor area (SMA); left and right primary motor cortex (M1); left and right anterior intraparietal sulcus (aIPS); left and right superior parietal lobule (SPL); left and right superior parieto-occipital cortex (SPOC); left and right lateral occipito-temporal cortex (LOTC).

3.2.2 Time-resolved ROI-MVPA. To examine the temporal unfolding of movement decoding for the different tasks in selected brain regions we ran the ROI-MVPA with a time-resolved approach (i.e., classification performed separately at each acquired volume, starting from the onset of an event) (Fig. 4-6). For each ROI in Fig. 4-6, the overlapping line plots represent the classification accuracy to distinguish between reach-to-touch and reach-to-grasp movements (expressed in percentage correct) at each time-point for the different conditions. On the left column, the x-axis is time-locked to the onset of the visual/auditory instructing cue (0-2 s/vol. 1). The yellow line refers to decoding of movement type for delayed planning (collapsed across go and no-go trials), the bright green line to decoding of movement type for non-delayed execution and the blue line to the decoding of movement type across conditions with and without a delay (i.e., training the classifier on delayed planning using non-delayed execution for testing, and vice versa). On the right column, the x-axis is time-locked to the go/no-go cue (0-2 s/vol. 1). The dark green line refers to decoding for delayed execution, and the red line to decoding for delayed suppression (i.e., after the no-go cue). The bright green line is identical to the one presented in the left column and serves for ease of comparison between decoding results across conditions. Fig. 4 shows the results in bilateral frontal motor regions, Fig. 5 in bilateral parietal sensorimotor regions, and Fig. 6 in bilateral fronto-temporal ventral stream regions. During the planning phase of delayed trials (i.e., yellow line plots) we observed significant decoding of movement type in L-PMd at 4-6 s (vol. 3; Fig. 4), L-aIPS at

< Fig. 4, 1.5 columns >

2-4 s (vol. 2; Fig. 5), and L-SPL at 8-10 s (vol. 5; Fig. 5). Results for delayed and non-delayed execution (i.e., dark and bright green line plots) were very similar: significant decoding started as early as 4-6 s (vol. 3) and continued until as late as 10-12 s (vol. 6) in bilateral M1, PMd, SMA, and aIPS. For the no-go task (i.e., red line plots) we observed some trends in L-PMd at 2-4 s (vol. 2), L-SMA at 2-6 s (vol. 2-3), and L-dlPFC at 2-4 s (vol. 2), but none of these survived correction for multiple comparisons. Regarding shared representations across delayed and non-delayed movement plans (i.e., blue line plots), we were able to decode movement types across delay conditions at 2-4 s (vol. 2) in L-M1.

< Fig. 5, 1.5 columns >

< Fig. 6, 1.5 columns >

3.2.3 Time-resolved searchlight-MVPA. The time-resolved searchlight-based MVPA (Supplementary Fig. 2-3) was intended to provide a whole-brain overview of regions discriminating between reach-to-touch and reach-to-grasp movements, including regions not specifically covered by the ROI analysis. Given the number of voxels in the brain, multiple comparison correction is a known limiting factor for power in searchlight analyses (Etzel et al., 2013; Stelzer et al., 2013; Ariani et al., 2015). However, despite overall weaker results, decoding trends were largely in line with those observed in the ROIs.

4. DISCUSSION

To examine how movement representations evolve throughout different stages of planning, execution, and suppression, we compared three tasks in which movements were (1) planned, withheld, and then executed (delayed go task); (2) planned and immediately executed (non-delayed go task); or (3) planned, withheld, and then suppressed (delayed no-go task). We found transient representations of movement plans in parieto-frontal regions and shared representations across delayed and immediate movement plans in human M1. In the following, we discuss the main findings in more detail.

4.1 Shared early neural representations for delayed and non-delayed movement plans

We obtained significant cross-condition decoding between delayed planning and non-delayed execution in the left primary motor cortex at 2-4 s (vol. 2; Fig. 4). In other words, during early stages of movement planning, representations of reach-to-touch and reach-to-grasp movements are similar to the representations obtained during early stages of immediate movement execution (i.e., movements that are not preceded by a delay). Admittedly, our experiment was not designed to disentangle whether these representations reflect a more abstract level of movement planning (e.g., goals and intentions) or a more concrete level of movement programming (e.g., muscle force or joint angles). Rather, we argue that they constitute a common thread for planned movements that do not depend on the presence of a delay. Early neuropsychology and behavioral evidence suggested distinct cortical pathways for memory-driven and immediate actions (Hu et al., 1999; Milner et al., 2001, 2003; Goodale et al., 2004; Rossit et al., 2010; but see, Himmelbach and Karnath, 2005; Franz et al., 2009; Hesse and Franz, 2009; Himmelbach et al., 2009; Fiehler et al., 2011). In highlighting a convergence between delayed and non-delayed movement plans (at the level of neural representations), our data are in line with results by Fiehler et al. (2011), which demonstrated that overlapping clusters of voxels in human primary motor cortex and dorsal premotor cortex are recruited during the planning phase and immediate execution of grasping movements. Our findings also extend the results by Crammond and Kalaska (2000) and Ames et al. (2014), which show that macaque primary motor cortex contains neural representations of planned movements that are shared across delayed and non-delayed contexts, to the early

phases of delayed planning and immediate execution in human primary motor cortex. In humans, brain responses to movement execution are generally much stronger than those obtained during planning delays (Gallivan et al., 2011b; Ariani et al., 2015). The fact that we failed to obtain significant cross-condition decoding between delayed planning and immediate execution in most regions and at most time points in the presence of within-condition decoding suggests that also the corresponding multi-voxel activity patterns tend to differ. Churchland, Shenoy, and colleagues were the first to point out a non-trivial relationship between preparatory and movement-related activity (Churchland et al., 2010; Shenoy et al., 2013; Kaufman et al., 2014), showing low correlations between the two at least at the level of neuronal populations. More recently, Elsayed et al. (2016) found that at the level of neuronal populations in monkey M1 and PMd patterns of responses for preparatory and movement computations were qualitatively different. Yet, preparatory activity patterns could be used to predict the upcoming movement activity patterns, just before movement onset. To resolve the apparent controversy the authors hypothesized the existence of different but tightly linked computations: a short temporal overlap between preparatory and movement activities would allow the state of the neuronal population to transition from preparation to execution (Elsayed et al., 2016). In line with this view, the time-resolved MVPA approach used in the current study revealed shared representations between early stages of delayed planning and immediate execution, i.e., before brain activity begins to diverge both in terms of overall activation and activity patterns.

One potential reservation could be that cross-condition decoding is driven by the sensory properties of the instructing cues (e.g., stimulus-response mapping). However, since we chose different modalities for instruction cues in the delayed (visual) and the non-delayed (auditory) task, we consider this explanation unlikely, unless one assumes that primary motor cortex contains multi-modal (audio-visual) representations of sensory stimuli. Another potential reservation when interpreting the significant cross-condition decoding in L-M1 at 2-4 s (vol. 2) derives from the fact that for the within-condition decoding (delayed planning, non-delayed execution) we obtained trends in the searchlight analysis (Supplementary Fig. 2B, vol. 2), but no effects that survived correction for multiple comparisons in the ROI analysis (Fig. 4, upper left panel). A possible explanation for this seeming discrepancy is the fact that

more trials can be used for training and testing the classifier for cross-decoding (i.e., train on all delayed planning trials, and test on all non-delayed trials, and vice versa), whereas within-condition decoding has to rely on half of the trials (e.g., train and test on delayed planning trials only). Moreover, it is worth mentioning that several previous studies reported similar observations, i.e., stronger cross-condition decoding than within-condition decoding (Gallivan et al., 2011b, 2013; Oosterhof et al., 2012; Ariani et al., 2015).

4.2 Planning vs stimulus-response (S-R) mapping

Extending previous reports that used more conventional MVPA (Gallivan et al., 2011a, 2013; Ariani et al., 2015), we obtained significant decoding of hand movements during delayed planning in premotor (L-PMd) and parietal (L-aIPS) cortex, using time-resolved MVPA (Fig. 4-5). One might argue that these results could be partially driven by decoding of (1) the instructing color cues or (2) the S-R mapping rather than movement planning. However, first, our regions of interest are not part of the inferior temporal neural networks typically associated with color perception, or knowledge about colors (Martin et al., 1995; Simmons et al., 2007); second, we recently compared internally and externally triggered movements and found, both in L-PMd and L-aIPS, representations of planned hand movements that generalized across the two conditions and thus did not depend on any specific instruction cue (Ariani et al., 2015). In agreement with previous studies (Cavina-Pratesi, 2006; Hartstra et al., 2012), this suggests that representations in dorsal premotor and anterior intraparietal regions are indeed driven by movement planning rather than by S-R mapping.

4.3 The role of visual feedback

The lack of within-condition decoding for planned movement types in visual or visuomotor areas such as LOTC, SPOC, and PMv might seem surprising given recent reports by Gallivan and colleagues (Gallivan et al., 2013a, 2013c, 2015). This discrepancy might stem from the role of visual feedback in decoding movement plans. In contrast to the studies by Gallivan et al. (2013a, 2013c, 2015), participants in the current study had no direct viewing of the target object, or their own hands, throughout the entire experimental session. We explicitly chose to use non-visually guided actions in the attempt to disentangle visual and motor components

during movement planning. It is possible that the decoding of movement plans in areas such as LOTC, SPOC and PMv, which are known to contain visually driven neuronal populations, require sight of the movement, the object, or both. An alternative, non mutually exclusive, possibility is that the lack of decoding is related to limitations intrinsic to the method used here. For example, BOLD time-course data (sampled every TR) are a more variable estimate of the brain signal than beta-weights estimated for the entire duration of an event (collapsing across TRs). When using BOLD time-course data as input for the classifier, this variability might result in less robust decoding than conventional MVPA that is based on beta weights. This highlights the important trade-off between temporal resolution (time-resolved MVPA) and robustness of results (conventional MVPA).

4.4 Movement planning: sustained or transient neural process?

Significant time-resolved decoding appeared early within the planning delay (vol. 2 and vol. 3) and only lasted for one volume. This seems to suggest transient neural representations of movement plans in parieto-frontal regions, at least at the level of multivariate movement decoding (as opposed to univariate signal amplitude). Previous studies using delayed movements (Toni et al., 2001; Curtis et al., 2004; Lindner et al., 2010; Chapman et al., 2011; Gallivan et al., 2011b) suggested that planning is a sustained neural process that begins with an instructing cue and persists throughout the entire delay until the trigger cue. We consider it likely that the nature of the planning-related activity during the delay (transient vs sustained) varies as a function of the task demands (Mauritz and Wise, 1986). Studies with long, fixed planning delays could elicit a more sustained brain response, whereas studies with short, jittered delays could evoke a more transient response. Further studies, possibly using time-resolved decoding, are required to directly test these predictions.

4.5 Unspecific suppression of movement plans

Despite not being the main focus of this study, our design enabled us to also examine neural representations of suppressed movement plans. One possible outcome was that information about planned movements in multi-voxel patterns of fMRI activity is still present after a No-Go cue, meaning that some brain regions are involved in suppressing specific movement plans

(i.e., that these inhibitory signals are movement specific). An alternative possibility was that, regardless of the preceding movement plan, the No-Go cue would trigger unspecific suppression, similarly for different movement types, thus not allowing their decoding.

Despite some trends in L-dlPFC (vol. 2), L-PMd (vol. 2) and L-SMA (vol. 2-3), we failed to obtain significant decoding of suppressed movement plans at any time-point or ROI (Fig. 4-6). This outcome would be compatible with the view of unspecific suppression of movement plans, although null effects are hard to interpret. For instance, it could be that, due to poor spatio-temporal resolution, fMRI is not suitable for answering this research question (Dubois et al., 2015). Furthermore, the lack of significant decoding could be due to a statistical power issue intrinsic to time-resolved MVPA (i.e., decoding at separate time-points, thus inflating the number of comparisons that have to be corrected for).

Another possibility, one might argue, is that participants were not actively planning during No-Go trials, and thus had nothing to subsequently suppress. It should be noted, however, that the order of conditions within each run was pseudo-randomized. Since Go and No-Go trials were indistinguishable until the trigger cue appeared, participants could not know in advance whether or not they were in a No-Go trial (i.e., whether they would be later asked to suppress the planned movement or not). Thus, if the null-effect during movement suppression was due to a lack of planning in No-Go trials, then we should also have been unable to decode upcoming movements during the delay period of Go trials, which was not the case.

4.6 Conclusions and future directions

In agreement with previous work in non-human primates, we provided evidence for early shared representations between delayed and non-delayed movement plans in human primary motor cortex. Our findings were made possible by a time-resolved decoding approach that allowed us to examine the unfolding of movement representations across different stages of movement planning and generation, suggesting planning as a more transient process than previously hypothesized. Having demonstrated the general feasibility of this approach, we hope that this method will stimulate future research on the neural dynamics of the human prehension network.

ACKNOWLEDGEMENTS

This work was supported by the Provincia Autonoma di Trento and the Fondazione Cassa di Risparmio di Trento e Rovereto. We are thankful to Jens Schwarzbach for setting up the Arduino for response collection and to Hayley Prins for proofreading the manuscript. The authors declare no conflicts of interest.

REFERENCES

Afshar A, Santhanam G, Yu BM, Ryu SI, Sahani M, Shenoy K V. (2011) Single-trial neural correlates of arm movement preparation. Neuron 71:555–564.

Ames KC, Ryu SI, Shenoy K V. (2014) Neural dynamics of reaching following incorrect or absent motor preparation. Neuron 81:438–451.

Ariani G, Wurm MF, Lingnau A (2015) Decoding Internally and Externally Driven Movement Plans. Journal of Neuroscience 35:14160–14171.

Baumann MA, Fluet M-C, Scherberger H (2009) Context-Specific Grasp Movement Representation in the Macaque Anterior Intraparietal Area. Journal of Neuroscience 29:6436–6448.

Beurze SM, de Lange FP, Toni I, Medendorp WP (2009) Spatial and effector processing in the human parietofrontal network for reaches and saccades. Journal of Neurophysiology 101:3053–3062.

Bode S, Haynes JD (2009) Decoding sequential stages of task preparation in the human brain. NeuroImage 45:606–613.

Brainard DH (1997) The Psychophysics Toolbox. Spatial Vision 10:433–436.

Brandi M, Wohlschla A, Sorg C, Hermsdo J (2014) The Neural Correlates of Planning and Executing Actual Tool Use. Journal of Neuroscience 34:13183–13194.

Cavina-Pratesi C (2006) Dissociating Arbitrary Stimulus-Response Mapping from Movement Planning during Preparatory Period: Evidence from Event-Related Functional Magnetic Resonance Imaging. Journal of Neuroscience 26:2704–2713.

Chapman CS, Gallivan JP, Culham JC, Goodale MA (2011) Mental blocks: fMRI reveals top-down modulation of early visual cortex when obstacles interfere with grasp planning. Neuropsychologia 49:1703–1717.

Churchland MM, Cunningham JP, Kaufman MT, Ryu SI, Shenoy K V. (2010) Cortical Preparatory Activity: Representation of Movement or First Cog in a Dynamical Machine?

Neuron 68:387–400.

Churchland MM, Yu BM, Ryu SI, Santhanam G, Shenoy K V (2006) Neural variability in premotor cortex provides a signature of motor preparation. Journal of Neuroscience 26:3697–3712.

Cisek P, Kalaska JF (2004) Neural correlates of mental rehearsal in dorsal premotor cortex. Nature 431:993–996.

Cisek P, Kalaska JF (2005) Neural correlates of reaching decisions in dorsal premotor cortex: Specification of multiple direction choices and final selection of action. Neuron 45:801–814.

Crammond DJ, Kalaska JF (2000) Prior information in motor and premotor cortex: activity during the delay period and effect on pre-movement activity. Journal of Neurophysiology 84:986–1005.

Cui H, Andersen RA (2011) Different Representations of Potential and Selected Motor Plans by Distinct Parietal Areas. Journal of Neuroscience 31:18130–18136.

Curtis CE, Rao VY, D'Esposito M (2004) Maintenance of Spatial and Motor Codes during Oculomotor Delayed Response Tasks. Journal of Neuroscience 24:3944–3952.

Dubois J, de Berker AO, Tsao DY (2015) Single Unit Recordings in the Macaque Face Patch System Reveal Limitations of fMRI MVPA. Journal of Neuroscience 35:2791–2802.

Elsayed GF, Lara AH, Kaufman MT, Churchland MM, Cunningham JP (2016) Reorganization between preparatory and movement population responses in motor cortex. Nature Communications:13239.

Etzel JA, Zacks JM, Braver TS (2013) Searchlight analysis: Promise, pitfalls, and potential. NeuroImage 78:261–269.

Fabbri S, Caramazza A, Lingnau A (2010) Tuning curves for movement direction in the human visuomotor system. Journal of Neuroscience 30:13488–13498.

Fabbri S, Caramazza A, Lingnau A (2012) Distributed sensitivity for movement amplitude in

directionally tuned neuronal populations. Journal of Neurophysiology 107:1845–1856.

Fabbri S, Strnad L, Caramazza A, Lingnau A (2014) Overlapping representations for grip type and reach direction. NeuroImage 94:138–146.

Fiehler K, Bannert MM, Bischoff M, Blecker C, Stark R, Vaitl D, Franz VH, Rösler F (2011) Working memory maintenance of grasp-target information in the human posterior parietal cortex. NeuroImage 54:2401–2411.

Fluet M-C, Baumann M a, Scherberger H (2010) Context-Specific Grasp Movement Representation in Macaque Ventral Premotor Cortex. Journal of Neuroscience 30:15175–15184.

Franz VH, Hesse C, Kollath S (2009) Visual illusions, delayed grasping, and memory: no shift from dorsal to ventral control. Neuropsychologia 47:1518–1531.

Gallivan JP, Cavina-Pratesi C, Culham JC (2009) Is That within Reach? fMRI Reveals That the Human Superior Parieto-Occipital Cortex Encodes Objects Reachable by the Hand. Journal of Neuroscience 29:4381–4391.

Gallivan JP, Chapman CS, McLean DA, Flanagan JR, Culham JC (2013a) Activity patterns in the category-selective occipitotemporal cortex predict upcoming motor actions. European Journal of Neuroscience 38:2408–2424.

Gallivan JP, Culham JC (2015) Neural coding within human brain areas involved in actions. Current Opinion in Neurobiology 33:141–149.

Gallivan JP, Johnsrude IS, Flanagan JR (2015) Planning Ahead: Object-Directed Sequential Actions Decoded from Human Frontoparietal and Occipitotemporal Networks. Cerebral Cortex 26:1–23.

Gallivan JP, McLean DA, Flanagan JR, Culham JC (2013b) Where One Hand Meets the Other: Limb-Specific and Action-Dependent Movement Plans Decoded from Preparatory Signals in Single Human Frontoparietal Brain Areas. Journal of Neuroscience 33:1991–2008.

Gallivan JP, McLean DA, Smith FW, Culham JC (2011a) Decoding Effector-Dependent and Effector-Independent Movement Intentions from Human Parieto-Frontal Brain Activity. Journal of Neuroscience 31:17149–17168.

Gallivan JP, McLean DA, Valyear KF, Culham JC (2013c) Decoding the neural mechanisms of human tool use. eLife 2:e00425.

Gallivan JP, McLean DA, Valyear KF, Pettypiece CE, Culham JC (2011b) Decoding Action Intentions from Preparatory Brain Activity in Human Parieto-Frontal Networks. Journal of Neuroscience 31:9599–9610.

Gertz H, Fiehler K (2015) Human posterior parietal cortex encodes the movement goal in a pro-/anti-reach task. Journal of Neurophysiology 114:170–183.

Goodale MA, Westwood DA, Milner AD (2004) Two distinct modes of control for object-directed action. Progress in Brain Research 144:131–144.

Haggard P (2005) Conscious intention and motor cognition. Trends in Cognitive Sciences 9:290–295.

Haggard P (2008) Human volition: towards a neuroscience of will. Nature Reviews Neuroscience 9:934–946.

Harrison SA, Tong F (2009) Decoding reveals the contents of visual working memory in early visual areas. Nature 458:632–635.

Hartstra E, Waszak F, Brass M (2012) The implementation of verbal instructions: Dissociating motor preparation from the formation of stimulus-response associations. NeuroImage 63:1143–1153.

Heed T, Beurze SM, Toni I, Roder B, Medendorp WP (2011) Functional Rather than Effector-Specific Organization of Human Posterior Parietal Cortex. Journal of Neuroscience 31:3066–3076.

Hesse C, Franz VH (2009) Memory mechanisms in grasping. Neuropsychologia 47:1532–1545.

Himmelbach M, Karnath H (2005) Dorsal and ventral stream interaction: contributions from optic ataxia. Journal of Cognitive Neuroscience 17:632–640.

Himmelbach M, Nau M, Zundorf I, Erb M, Perenin MT, Karnath HO (2009) Brain activation during immediate and delayed reaching in optic ataxia. Neuropsychologia 47:1508–1517.

Hu Y, Eagleson R, Goodale MA (1999) The effects of delay on the kinematics of grasping. Experimental Brain Research 126:109–116.

Hwang EJ, Andersen RA (2009) Brain Control of Movement Execution Onset Using Local Field Potentials in Posterior Parietal Cortex. Journal of Neuroscience 29:14363–14370.

Kaufman MT, Churchland MM, Ryu SI, Shenoy KV (2014) Cortical activity in the null space: permitting preparation without movement. Nature Neuroscience 3:440–448.

Kriegeskorte N, Simmons WK, Bellgowan PSF, Baker CI (2009) Circular analysis in systems neuroscience: the dangers of double dipping. Nature Neuroscience 12:535–540.

Leoné FTM, Heed T, Toni I, Medendorp WP (2014) Understanding effector selectivity in human posterior parietal cortex by combining information patterns and activation measures. Journal of Neuroscience 34:7102–7112.

Linden DEJ, Oosterhof NN, Klein C, Downing PE (2012) Mapping brain activation and information during category-specific visual working memory. Journal of Neurophysiology 107:628–639.

Lindner A, Iyer A, Kagan I, Andersen RA (2010) Human posterior parietal cortex plans where to reach and what to avoid. The Journal of Neuroscience 30:11715–11725.

Lingnau A, Downing PE (2015) The lateral occipitotemporal cortex in action. Trends in Cognitive Sciences 19:268–277.

Mars RB, Coles MGH, Hulstijn W, Toni I (2008) Delay-related cerebral activity and motor preparation. Cortex 44:507–520.

Martin A, Haxby J V, Lalonde FM, Wiggs CL, Ungerleider LG (1995) Discrete cortical regions

associated with knowledge of color and knowledge of action. Science (New York, NY) 270:102–105.

Mauritz KH, Wise SP (1986) Premotor cortex of the rhesus monkey: neuronal activity in anticipation of predictable environmental events. Experimental Brain Research 61:229–244.

Milner AD, Dijkerman HC, McIntosh RD, Rossetti Y, Pisella L (2003) Delayed reaching and grasping in patients with optic ataxia. Progress in Brain Research 142:225–242.

Milner AD, Dijkerman HC, Pisella L, McIntosh RD, Tilikete C, Vighetto A, Rossetti Y (2001) Grasping the past. delay can improve visuomotor performance. Current Biology 11:1896–1901.

Oosterhof NN, Connolly AC, Haxby J V. (2016) CoSMoMVPA: Multi-Modal Multivariate Pattern Analysis of Neuroimaging Data in Matlab/GNU Octave. Frontiers in Neuroinformatics 10:273389–27.

Oosterhof NN, Tipper SP, Downing PE (2012) Visuo-motor imagery of specific manual actions: A multi-variate pattern analysis fMRI study. NeuroImage 63:262–271.

Pertzov Y, Avidan G, Zohary E (2011) Multiple reference frames for saccadic planning in the human parietal cortex. Journal of Neuroscience 31:1059–1068.

Raos V (2004) Functional Properties of Grasping-Related Neurons in the Dorsal Premotor Area F2 of the Macaque Monkey. Journal of Neurophysiology 92:1990–2002.

Rossit S, Szymanek L, Butler SH, Harvey M (2010) Memory-guided saccade processing in visual form agnosia (patient DF). Experimental Brain Research 200:109–116.

Scheperjans F, Eickhoff SB, Hömke L, Mohlberg H, Hermann K, Amunts K, Zilles K (2008) Probabilistic maps, morphometry, and variability of cytoarchitectonic areas in the human superior parietal cortex. Cerebral Cortex 18:2141–2157.

Schwarzbach J (2011) A simple framework (ASF) for behavioral and neuroimaging experiments based on the psychophysics toolbox for MATLAB. Behavior Research

Methods 43:1194–1201.

Shenoy K V, Sahani M, Churchland MM (2013) Cortical control of arm movements: a dynamical systems perspective. Annual Review of Neuroscience 36:337–359.

Simmons WK, Ramjee V, Beauchamp MS, McRae K, Martin A, Barsalou LW (2007) A common neural substrate for perceiving and knowing about color. Neuropsychologia.

Singhal A, Monaco S, Kaufman LD, Culham JC (2013) Human fMRI reveals that delayed action re-recruits visual perception. PloS One 8:e73629.

Soon CS, Brass M, Heinze H-J, Haynes J-D (2008) Unconscious determinants of free decisions in the human brain. Nature Neuroscience 11:543–545.

Stelzer J, Chen Y, Turner R (2013) Statistical inference and multiple testing correction in classification-based multi-voxel pattern analysis (MVPA): random permutations and cluster size control. NeuroImage 65:69–82.

Toni I, Thoenissen D, Zilles K (2001) Movement preparation and motor intention. NeuroImage 14:S110–S117.

Townsend BR, Subasi E, Scherberger H (2011) Grasp Movement Decoding from Premotor and Parietal Cortex. Journal of Neuroscience 31:14386–14398.

Verhagen L, Dijkerman HC, Grol MJ, Toni I (2008) Perceptuo-Motor Interactions during Prehension Movements. Journal of Neuroscience 28:4726–4735.

Verhagen L, Dijkerman HC, Medendorp WP, Toni I (2012) Cortical Dynamics of Sensorimotor Integration during Grasp Planning. Journal of Neuroscience 32:4508–4519.

Verhagen L, Dijkerman HC, Medendorp WP, Toni I (2013) Hierarchical Organization of Parietofrontal Circuits during Goal-Directed Action. Journal of Neuroscience 33:6492–6503.

Wise, SP, Kurata, K (1989) Set-related activity in the premotor cortex of rhesus monkeys: effect of triggering cues and relatively long delay intervals. Somatosensory & Motor Research. 6(5-6):455–476.

FIGURE CAPTIONS

Figure 1. Experimental setup, design, and timing. A. View of the setup from the side. Unimanual right-handed movements were performed towards a target object mounted on a plexiglas workspace positioned at waist level. The wooden graspable object was composed of two small cuboids glued to each other (2 x 2 x 1 cm and 7 x 7 x 2 cm). Participants lied horizontally and maintained fixation on a screen that was visible binocularly through a mirror attached to the head coil (line of sight illustrated by black dashed line). This setup prevented visual feedback from the target object, or the participants' own movements (see also Ariani et al., 2015). **B.** Screenshots from video recordings to illustrate movement types. Whenever at rest participants were required to keep their right hand in the home position (closed in a fist and pressing the response buttons, left panel; see also A). The two movement types were reach-to-touch (no hand preshaping, central panel) and reach-to-grasp (whole-hand grip, right panel). **C.** Task types with respective trial timing. Every trial began with a brief flashing of the fixation cross (alert cue, 500 ms). In the delayed task a color cue (500 ms) instructed which of the two movements to prepare. Stimulus-response mappings (lower right corner) were counterbalanced across participants. Visual cues were followed by a jittered planning delay (2-14 s = delayed trials 8-14 s + catch trials 2-6 s) after which a go cue (dark fixation) prompted participants to perform the instructed movement (execution phase, 2 s). The reappearance of the grey fixation signaled to return to the home position and wait for the next trial (ITI 2-10 s, determined by Optseq2). In the non-delayed task the movement to perform was instructed via auditory cues (upward arrow = high-pitch sound; downward arrow = low-pitch sound) and there was no planning delay (i.e., sound simultaneous to the go cue). The no-go task was identical to the delayed task but, instead of the go cue, the fixation would briefly turn red (500 ms, no-go cue), indicating to suppress the previously planned movement. Both task and movement types were pseudorandomized within each functional run.

Figure 2. Regions of interest (ROIs). Black circles represent approximate locations of group-defined ROIs involved in movement generation. Actual ROIs used in the ROI-MVPA were defined, individually for each participant, as spheres (10mm radius) around individual peak voxels coming from single-subject statistical maps of the univariate contrast [delayed planning + non-delayed execution > baseline] (collapsing across movement types). For additional details, see Materials and Methods section and Table 1. All the other figure conventions are the same as in Supplementary Fig. 1.

Figure 3. Illustration of time-resolved ROI-MVPA procedures (hypothetical data). A. Normalized volume time-course (VTC) of the BOLD signal (arbitrary units) for one voxel of an example ROI, in one run of an example participant. For each trial of each example condition (e.g., Reach plan, green; Grasp plan, blue) we selected 5 volumes (e.g., for the planning of delayed task) starting from the onset of the condition. **B.** Dataset matrix of samples (volumes x movements x runs) x features (N voxels in the ROI). **C.** Leave-one-run-out cross-validation on multi-voxel patterns of fMRI data for the first volume of each condition (vol. 1). The training dataset (e.g., runs 1 to 9) was used to define a linear decision boundary in the feature space. The independent test dataset (run 10) was used for classification, whose outcome could only be binary (i.e., either 100%, or 0% correct). This procedure was repeated for 10 iterations, using all possible combinations of train and test runs. **D.** Mean decoding accuracy of the two conditions for each volume from cue onset resulting from the average of all cross-validation iterations. Given the binary nature of each classification outcome, the chance level was set at

50%.

Figure 4. Time-resolved ROI-MVPA in bilateral frontal motor regions. Mean percentage decoding accuracy of movements at each time-point (TR = 2 s) in selected ROIs (for details see Supplementary Figure 2 and Table 1). For each ROI, line plots on the left panel are time-locked to the onset of the visual instructing cue in the delayed task (D Plan, yellow), the auditory instructing cue in the non-delayed task (ND Exe, bright green), or both instructing/go audio-visual cues for the cross-condition decoding (Cross D-ND, blue). On the right panel, line plots are time-locked to the onset of the go cue for the delayed execution (D Exe, dark green) and the non-delayed execution (ND Exe, bright green), or the onset of the no-go cue for the no-go task (D No-Go, red). Please note that the bright green line is identical for the two sides of the line plot and was intended to facilitate direct comparison across conditions. Error bars represent within-subject standard error of the mean (SEM). Statistical significance was assessed via one-sample *t*-tests against 50% chance (grey horizontal line in each ROI plot) at each time-point separately. Results were corrected for multiple comparisons (number of time-points x number of ROIs) using TFCE (asterisk = uncorrected $p < 0.05$; star = TFCE corrected at $p < 0.05$).

Figure 5. Time-resolved ROI-MVPA in bilateral parietal sensorimotor regions. Legend and figure conventions are the same as in Fig. 4.

Figure 6. Time-resolved ROI-MVPA in bilateral fronto-temporal ventral stream regions. Legend and figure conventions are the same as in Fig. 4.

SUPPLEMENTARY MATERIAL

< Supplementary Fig. 1 >

Supplementary Figure 1. Univariate RFX-GLM analysis (N = 24). A. Univariate contrast [delayed planning > baseline], collapsing across movement types and go/no-go trials. **B.** Univariate contrast [non-delayed execution > baseline], collapsing across movement types. **C.** Univariate contrast [delayed no-go > delayed go], collapsing across movement types. All statistical group-maps were corrected for multiple comparisons using Threshold Free Cluster Enhancement (TFCE) as implemented in CoSMoMVPA (Oosterhof et al., 2016), thresholded at $p < 0.05$ and projected on the group-aligned inflated surface mesh for visualization purposes. White lines on the surface meshes denote main sulci as landmarks (see legend at the bottom of the figure).

< Supplementary Fig. 2 >

Supplementary Figure 2. Time-resolved whole-brain searchlight-MVPA for delayed and non-delayed tasks. Decoding procedures were identical to the ones used for the ROI-MVPA except for the use of a spherical searchlight (~250 voxels) approach (see *Materials and Methods*). Group (N = 24) mean decoding accuracy (in %, top) and uncorrected *t*-scores (bottom) whole-brain maps projected on the group-averaged surface mesh are shown at each time-point for within-condition decoding **(A, B)** and cross-condition decoding **(C)**. Accuracy maps, intended for descriptive purposes only, have different accuracy ranges across conditions. All *t*-maps are thresholded at $t = 2$. Clusters surviving TFCE correction for multiple comparisons ($p < 0.05$) are outlined in black. White lines on the surface meshes denote main sulci (same as in Supplementary Figures 1-2). **A.** Delayed Planning. Whole-brain maps are time-locked to the onset of the visual instructing cue (0-2 s/vol. 1). Due to jittered planning delays the earliest possible go or no-go signal was after 8 seconds (4 volumes). **B.** Non-delayed execution. Whole-brain maps are time-locked to the auditory instructing/go cue (0-2 s/vol. 1). **C.** Cross-condition decoding. Whole-brain maps are time-locked to both visual (for delayed planning) and auditory (for non-delayed execution) cues (0-2 s/vol. 1).

< Supplementary Fig. 3 >

Supplementary Figure 3. Time-resolved whole-brain searchlight-MVPA for delayed and no-go tasks. All figure conventions are the same as in Supplementary Figure 2. **A.** Delayed execution. Whole-brain maps are time-locked to the onset of the Go cue (0-2 s/vol. 1) for delayed trials only. **B.** Delayed suppression. Whole-brain maps are time-locked to the onset of the No-Go cue (0-2 s/vol. 1).

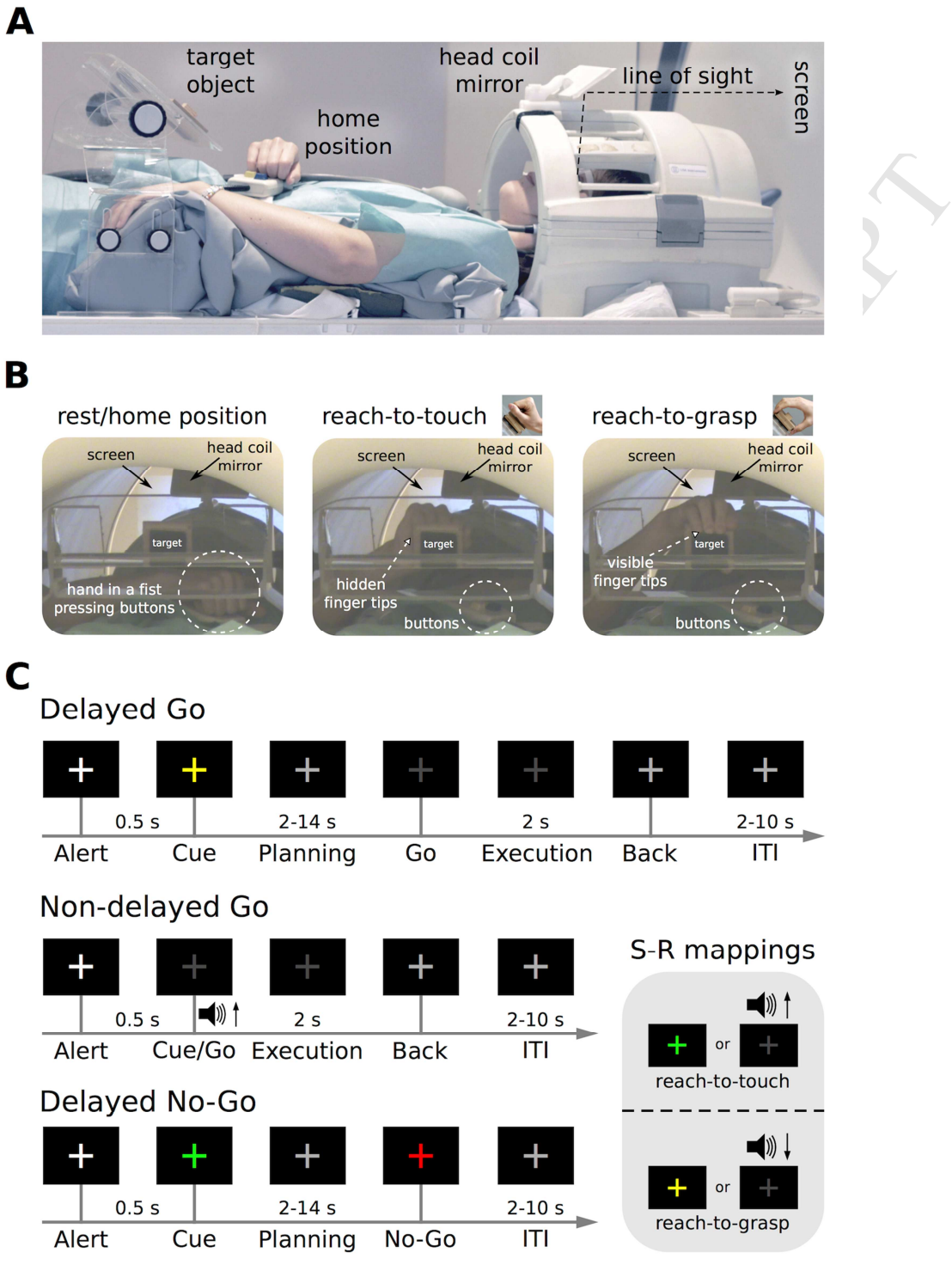
A
target object
home position
head coil mirror
line of sight
screen
B
rest/home position
reach-to-touch
reach-to-grasp
screen
head coil mirror
target
hand in a fist pressing buttons
hidden finger tips
buttons
visible finger tips
C
Delayed Go
0.5 s
2-14 s
2 s
2-10 s
Alert
Cue
Planning
Go
Execution
Back
ITI
Non-delayed Go
Cue/Go
Delayed No-Go
No-Go
S-R mappings
or
reach-to-touch
reach-to-grasp

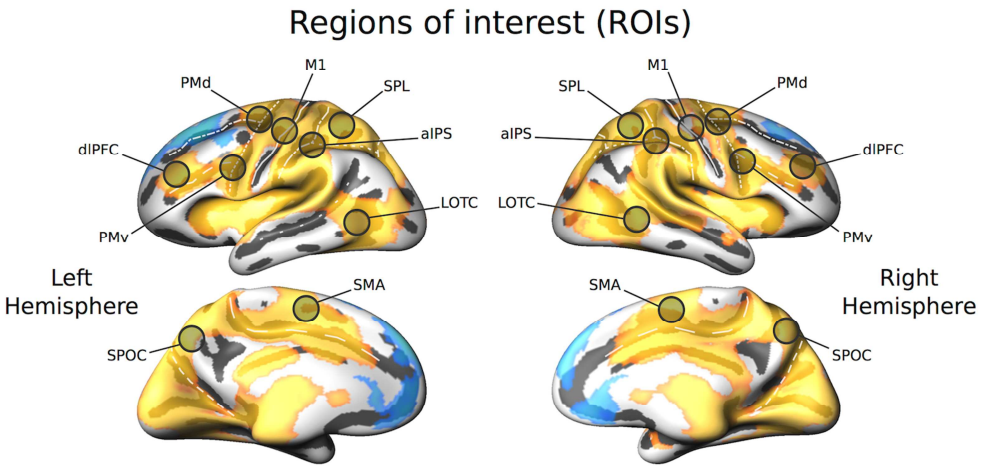

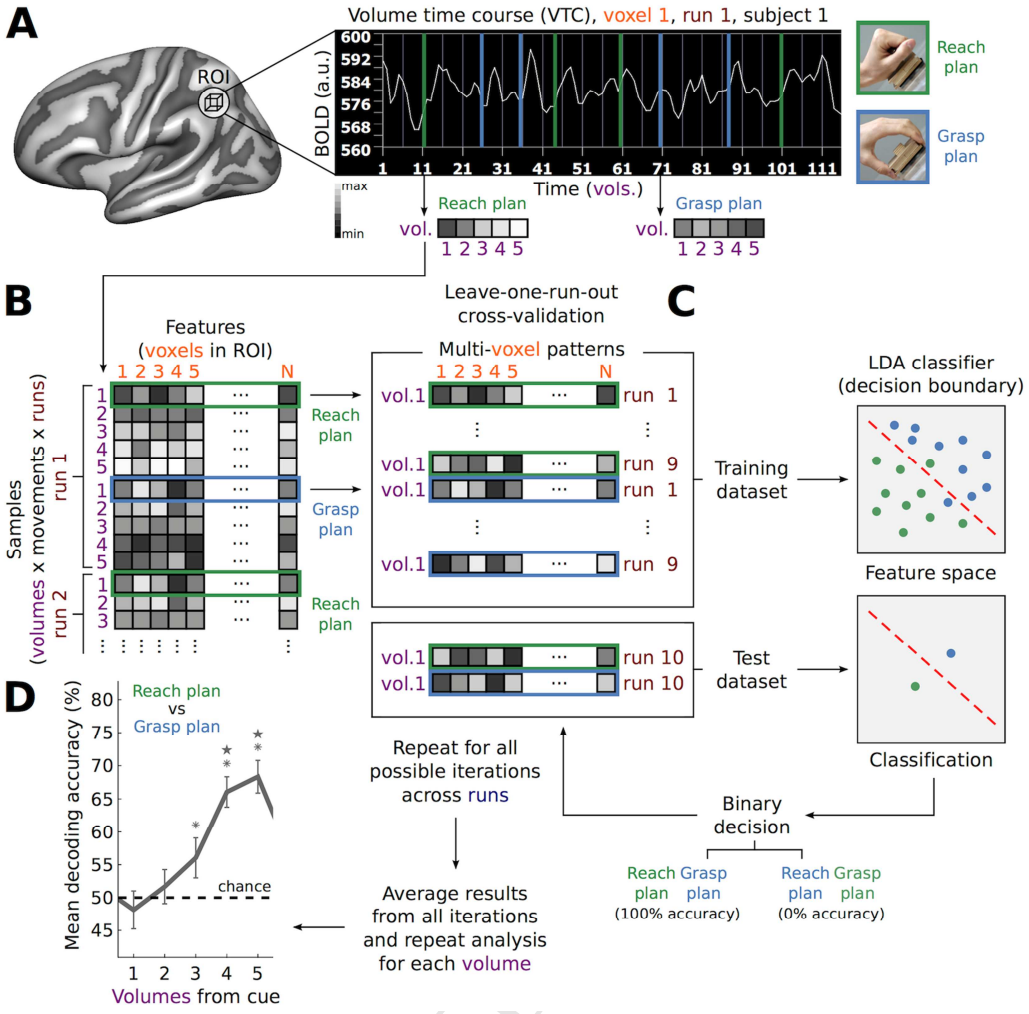

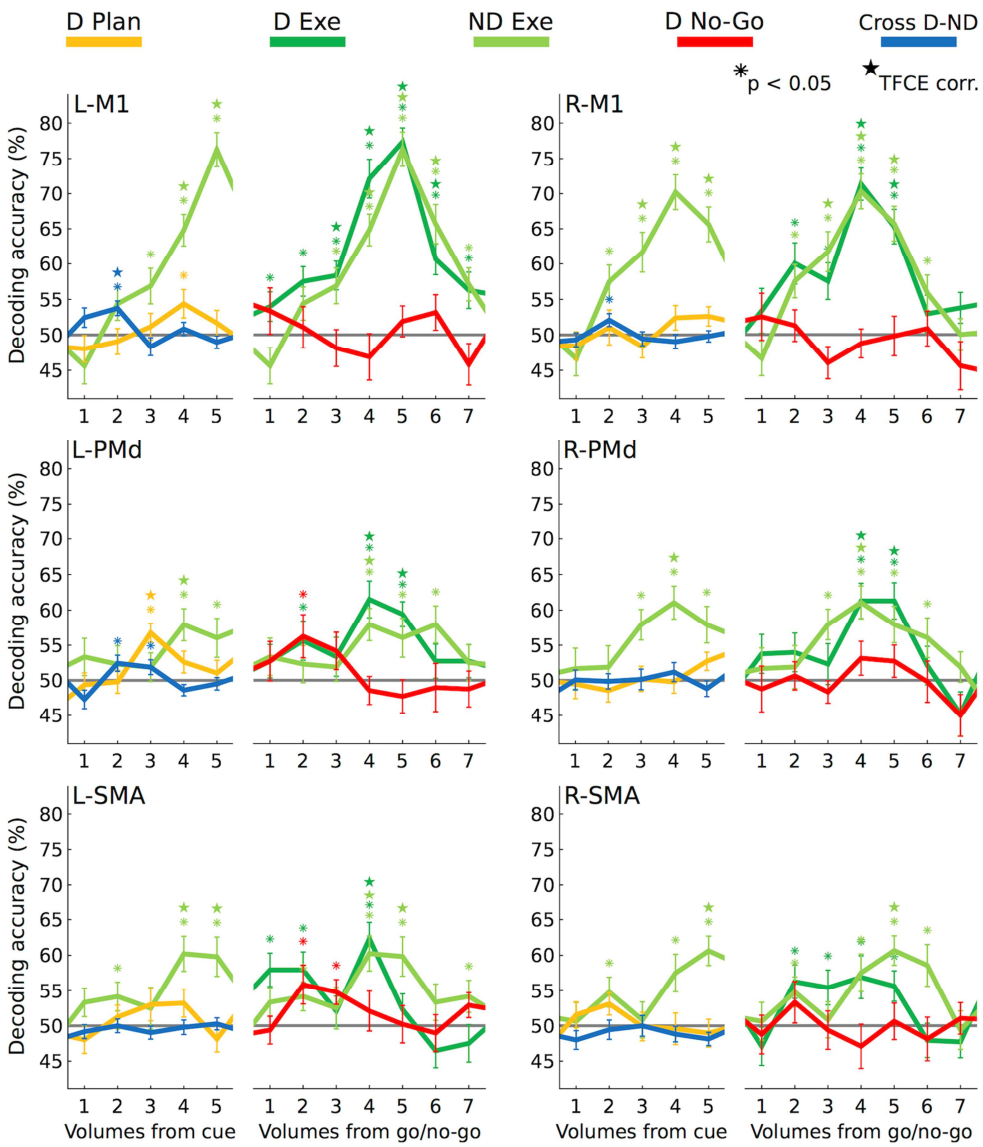
D Plan
D Exe
ND Exe
D No-Go
Cross D-ND
*p < 0.05
★TFCE corr.
L-M1
R-M1
L-PMd
R-PMd
L-SMA
R-SMA
Decoding accuracy (%)
Volumes from cue
Volumes from go/no-go

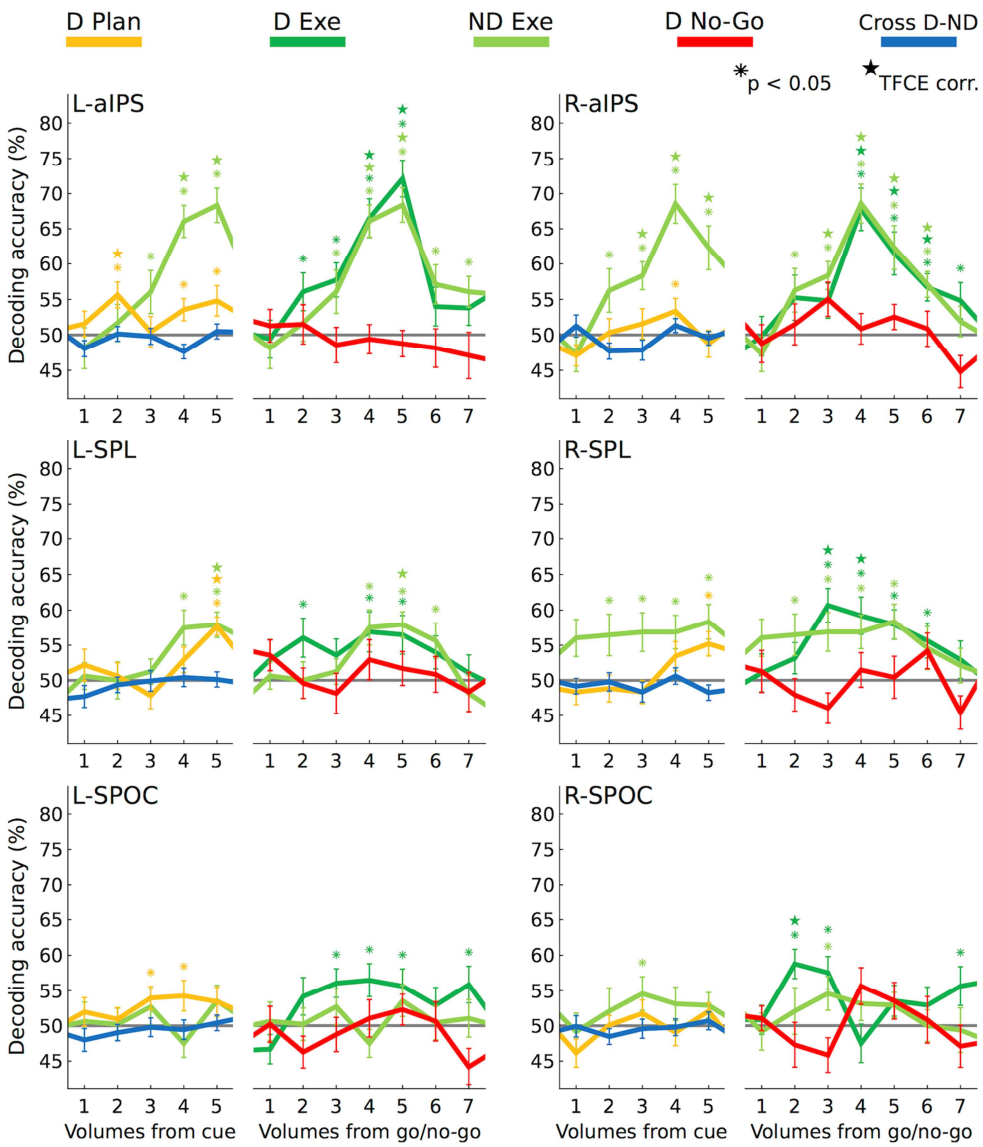
D Plan
D Exe
ND Exe
D No-Go
Cross D-ND
*p < 0.05
★TFCE corr.
L-aIPS
R-aIPS
L-SPL
R-SPL
L-SPOC
R-SPOC
Decoding accuracy (%)
Volumes from cue
Volumes from go/no-go

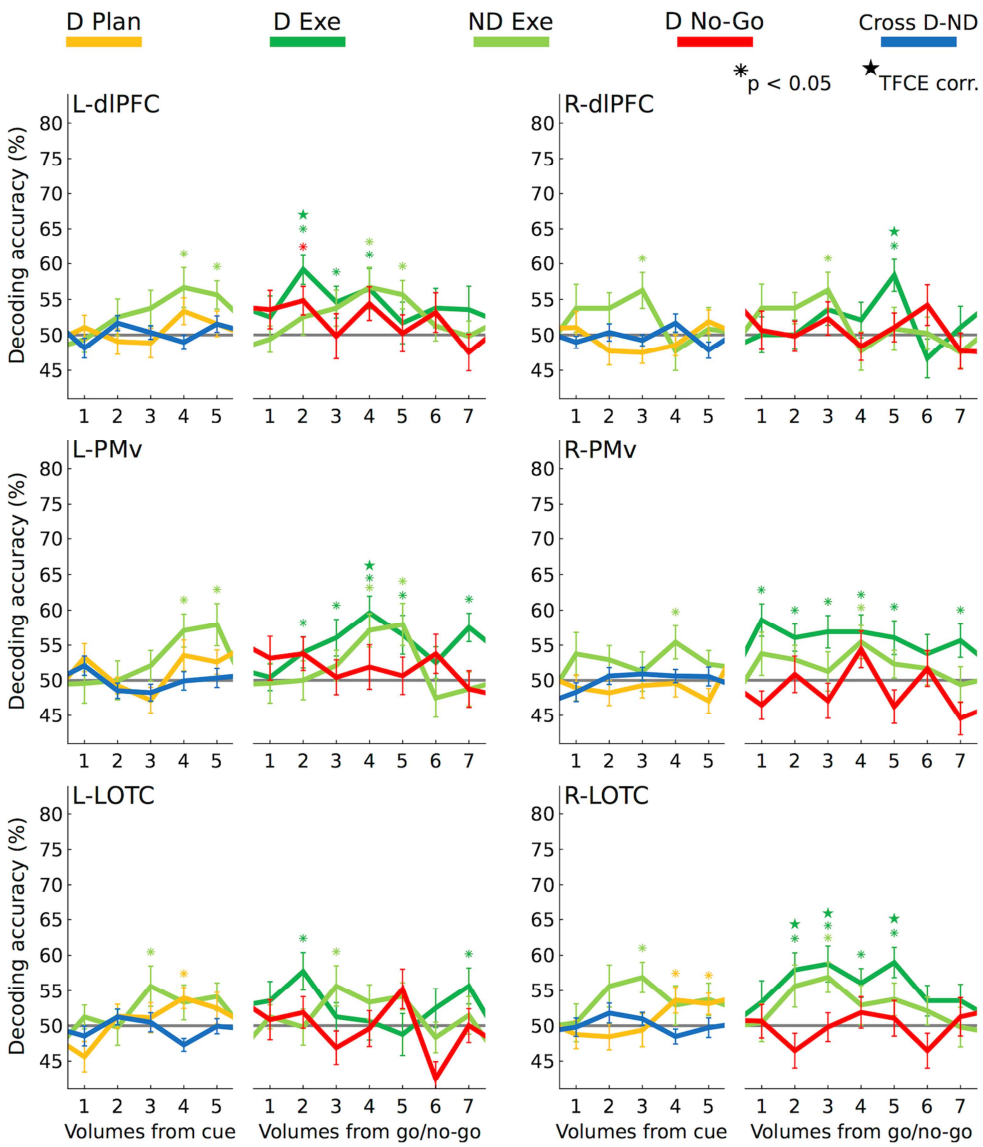
D Plan
D Exe
ND Exe
D No-Go
Cross D-ND
*p < 0.05
★TFCE corr.
L-dlPFC
R-dlPFC
L-PMv
R-PMv
L-LOTC
R-LOTC
Decoding accuracy (%)
Volumes from cue
Volumes from go/no-go